FULL PAPER

ADVANCED
FUNCTIONAL
MATERIALS
www.afm-journal.d

Check for
updates

Recapitulating Pancreatic Tumor Microenvironment through Synergistic Use of Patient Organoids and Organ-on-a-Chip Vasculature

Benjamin Fook Lun Lai, Rick Xing Ze Lu, Yangshuo Hu, Locke Davenport Huyer, Wenkun Dou, Erika Yan Wang, Nikolina Radulovich, Ming Sound Tsao, Yu Sun, and Milica Radisic*

Tumor progression relies on the interaction between neoplastic epithelial cells and their surrounding stromal partners. This cell cross-talk affects stromal development, and ultimately the heterogeneity impacts drug efficacy. To mimic this evolving paradigm, 3D vascularized pancreatic adenocarcinoma tissue is microengineered in a tri-culture system composed of patient-derived pancreatic organoids, human fibroblasts, and endothelial cells on a perfusable platform, situated in a 96-well plate. Through synergistic engineering, the benefits of cellular fidelity of patient tumor organoids are combined with the flow control of an organ-on-a-chip platform. Validation of this platform includes demonstrating the growth of pancreatic tumor organoids by monitoring the change in metabolic activity of the tissue. Investigation of the tumor microenvironment highlights the role of fibroblasts in symbiosis with patient organoids, resulting in a six-fold increase of collagen deposition and corresponding increase in tissue stiffness in comparison to fibroblast free controls. The value of a perfusable vascular network is evident in drug screening, as perfusing gemcitabine into stiffened matrix does not show the dose-dependent effects on decrease in tumor viability as those under static conditions. These findings demonstrate the importance of a dynamic synergistic relationship between patient cells with stromal fibroblasts, in a 3D perfused vascular network, to accurately recapitulate a dynamic tumor microenvironment.

1. Introduction

Pancreatic ductal adenocarcinoma (PDAC) is the most common form of pancreatic cancer and the fourth leading cause of cancer-associated mortality worldwide. PDAC results in extremely poor survival rates, of approx. 6 months from the time of diagnosis, averaging only 8% in a 5-year survival rate.[1] Despite multimodal efforts directed at improving PDAC drug efficacy, prognosis remains remarkably poor for these pancreatic cancer patients. Gemcitabine is regularly used as the first-line of treatment for PDAC patients but its use as a single agent often has little impact on patient survival.[2] Although the combination effect of gemcitabine with FOLFIRINOX improves survival in patients with advanced pancreatic cancer, this chemotherapy regimen shows limited progress in metastatic setting.[3] Development of drugs against novel genetic and epigenetic targets in the signalling pathway of pancreatic cancer cells or the PDAC microenvironment is therefore an active area for translational and clinical research.[4]

The poor prognosis occurs due to the frequently late diagnosis and the fact that PDAC often presents with a notably complex microenvironment that complicates treatment. The resilient nature of PDAC stems from its ever-evolving desmoplastic stroma.[5] In this heterogeneous microenvironment, the intercellular interactions between different stromal, normal epithelial, and cancer cells become disoriented to accommodate reorganization into a tumorigenic niche.[5]

B. F. L. Lai, R. X. Z. Lu, L. Davenport Huyer, E. Y. Wang, Prof. Y. Sun, Prof. M. Radisic
Institute of Biomaterials and Biomedical Engineering
University of Toronto
Toronto, Ontario, Canada
E-mail: m.radisic@utoronto.ca

Y. Hu, L. Davenport Huyer, Prof. M. Radisic
Department of Chemical Engineering and Applied Chemistry
University of Toronto
Toronto, Ontario, Canada

The ORCID identification number(s) for the author(s) of this article can be found under https://doi.org/10.1002/adfm.202000545.

L. Davenport Huyer, Prof. M. Radisic
Toronto General Research Institute
University Health Network
Toronto, Ontario, Canada

W. Dou, Prof. Y. Sun
Material Science and Engineering
University of Toronto
Toronto, Ontario, Canada

N. Radulovich, Dr. M. S. Tsao
Princess Margaret Cancer Centre
University Health Network
Toronto, Ontario, Canada

**ADVANCED
SCIENCE NEWS**
www.advancedsciencenews.com

**ADVANCED
FUNCTIONAL
MATERIALS**
www.afm-journal.de

In addition to the tumor structures of epithelial origin, abundant desmoplasia makes up to 90% of the PDAC tumor volume.[6] This structure consists of a large number of vasculature-supported cancer associated fibroblasts that both secrete cytokines as well as extracellular matrix (ECM) contributing to tumor stroma.[7–9] Fibroblasts and the ECM were demonstrated previously to promote tumor survival and proliferation, directly through secretion of pro-inflammatory cytokines as well as indirectly by inhibiting transport of chemotherapeutics as well as T-cells that could contribute to cancer cell elimination.[10–16] Interestingly, the efforts to eliminate matrix secreting α-smooth muscle actin (α-SMA) positive fibroblasts from PDAC microenvironment did not result in expected inhibitory effects on cancer progression in pre-clinical and clinical studies, and in some cases, they correlated with the worsened survival outcome.[17,18] This motivated the development of sophisticated 3D cell culture systems that would enable one to better mimic tumor microenvironment in vitro for the purposes of drug discovery.

Notable recent studies report the effects resulting from the symbiotic interaction of stroma and cancer cells, including increased tumor survival, increased ECM deposition, and enhanced tissue stiffness in 3D culture models.[19–26] In some reports, a tri-culture of endothelial cells, stromal cells, and epithelial tumor cells as a spheroid model increased tumor cell drug resistance which highlights that the endothelium may play more than just a transport barrier role.[27–29] However, most of these studies rely on the use of human cancerous cell lines or rodent primary cells. Majority of the studies do not embody the complexity of the presence of all three important tumor microenvironmental components: tumor cells, stroma, and vasculature. Thus, many of these studies failed to recapitulate the original structural integrity of an in vivo tumor.

Recent advances in the field of organoids enable generation of epithelial organoids from a number of organs. Formed through self-organization, organoids are sophisticated structures that exhibit architectural and cellular features of the physiological comparatives. Representative organoid models of various epithelial systems have been reported, including stomach, small intestine, colon, liver, pancreas, brain, kidney, lung, and mammary gland.[30,31] In the study of cancers, tumor organoid models have been developed for breast, colon, and pancreas.[30] These advances enable us to increase the cellular fidelity of 3D systems to be employed in the studies of human disease or drug discovery. However, they are limited by the fact that a plurality of organoids is being exposed directly to the test molecules instead of delivered through a nearby lumen, and they cannot be easily instrumented to provide specific readouts. As we recently postulated, these limitations can be easily overcome relying on the techniques from the field of organ-on-a-chip engineering.[32]

To better recapitulate disease mechanisms, an ideal in vitro model that not only resembles the PDAC architecture but also integrates hallmarks of the PDAC desmoplastic stroma and vascular transport is a necessity. Here, we set out to develop a synergistic platform for studies of PDAC that combines the cellular fidelity of the human primary tumor organoids, with reproducibility and addressability of an organ-on-a-chip device. In addition, to mimic an evolving stroma as well as a perfusable vasculature network, we used non-transformed human cells.

The pancreatic tumor model was built in the plastic platform, Integrated Vasculature for Assessing Dynamic Events, termed InVADE, situated in a 96-well plate based organ-on-a-chip system created by hot embossing.[33] To achieve this, we micro-fabricated a vascular bio-scaffold that defines the vascular space and can support the self-assembly of various cells into a 3D tissue in the parenchymal space. Uniquely, this bio-scaffold spans across multiple compartments of a standard well plate to connect tissue chamber with an inlet well and an outlet well to drive perfusion. To eliminate the resistance to mass transfer of vascular bio-scaffold, we incorporated nano-pores and micro-holes into the polymer walls.

We show that, through use of the perfusable InVADE vasculature, we can facilitate the culture and growth of organoids derived from patient PDAC cells. By doing this, we were able to capture the synergistic effects of cancer organoids and fibroblasts when co-cultured in the same 3D system. Finally, by co-culturing patient derived pancreatic cancer organoids and stromal fibroblasts under a perfusable vascular system, we present the applicability of this biomimetic system in recapitulating the appreciable desmoplasia of the in vitro PDAC microenvironment and demonstrate its inhibitory effect on a known chemotherapeutic treatment.

2. Experimental Section

2.1. Microfabrication of Scaffold and Device Assembly

The process of microfabrication and assembly of the InVADE platform is described in detail elsewhere.[33] A summary of essential components of the micro-fabricated InVADE polymeric scaffold structure and assembly is provided in Figure S1, Supporting Information.

Master molds of the top, bottom, and base plate were designed using AutoCAD software and were microfabricated by standard soft lithography techniques with the negative photoresist SU-8 (Micro Chem). Polydimethylsiloxane (PDMS) (Dow Corning Corporation) was used for replica molding each of the SU8 master molds. PDMS molds for the top and bottom layers of scaffold were pressed onto a PDMS sheet and a glass slide, respectively. They were perfused with a highly elastic polyester material, poly (octamethylene maleate (anhydride) 1,2,4-butanetricaboxylate),[34] mixed with a porogen, poly (ethylene glycol) dimethyl ether, (Sigma Aldrich) at 60:40 w/w along with 5% w/w ultraviolet initiator (Iragcure 2959, Sigma). Poly (octamethylene maleate [anhydride] 1,2,4-butanetricaboxylate) was synthesized as described using the following conditions: equimolar content of acid and alcohol reactive groups, a 2:3 molar ratio of acid to anhydride, reaction temperature of 150 °C, and constant N_2 gas purge. Following overnight perfusion through the PDMS molds, the pre-polymer was UV-crosslinked and the crosslinked layers were removed from the molds. The top and bottom layers of the scaffold were then 3D-stamped together to achieve the tubular scaffold.

PDMS mold for the fabrication of base plate was plasma bonded onto a silicon wafer, and the features were captured onto a polystyrene sheet through hot-embossing (EVG520 Hot Embossing System). Tubular scaffolds were carefully positioned onto pre-designed well features on the polystyrene base

plate. Biocompatible polyurethane (GSP 1552-2, GS polymers) was used to bond the polystyrene base plate onto a bottomless 96-well plate (square-shaped well, Greiner Bio One), and baked at 80 °C for 2 h to ensure quick crosslinking of the polyurethane glue. The platform was treated with 70% ethanol for 1 h as sterilization process before cell culture work.

2.2. Cell Culture Maintenance

Human umbilical vein endothelial cells (HUVECs, ATCC CRL-1730) were cultured in endothelial growth medium (EGM2, PromoCell). Human dermal fibroblasts (FBs), a generous gift from Dr. Gordana Vunjak-Novakovic (Columbia University), were maintained in Dulbecco's modified Eagle Medium (DMEM, Gibco) supplemented with 10% fetal bovine serum (FBS), and 1% v/v penillicin–streptomycin. HUVECs were used up to passage 6 and FBs were cultured between passages 8 and 9. Both cell types were expanded separately and seeded from a culture of >80% confluency.

Patient-derived organoid (PDO) was obtained from Princess Margaret Living Biobank (PMLB, https://www.livingbiobank. ca/) under a protocol (REB# 18.5642.1) approved by the University Health Network Research Ethics Board (Toronto, ON). The PDO model (PMLB code: PPTO.46) was derived from a patient with pancreatic ductal adenocarcinoma tumor and was cultured in Matrigel (growth factor reduced, Corning 356231) as described previously.[35] The PDO model was authenticated to match allele repeat to that of parental tumor by short tandem repeat or to recapitulate patient histological feature through H&E and immunohistochemistry (Figure S2, Supporting Information). Quality control assessment was performed routinely by flow cytometry against CD326 (EpCAM marker) to ensure culture was free of contaminated cells such as fibroblasts. More than 99% of patient cells were positive for the epithelial marker. The organoid growth medium (OGM) was composed of Advanced DMEM/F12 (Gibco, 12634-010) supplemented with 1% B27 (Gibco, 17504-044), 1.25 mM N-acetyl-L-cysteine (Sigma, A9165), 10 nM Gastrin I (Sigma, SCP0152), 50 ng mL^{-1} human EFG (Corning, 354052), 100 ng mL^{-1} human FGF-10 (Peprotech, 100-26), 100 ng mL^{-1} human Noggin (Peprotech, 120-10C), 0.5 μM A83-01 (Tocris, 2939), 10 μM Y-27632 (Selleck Chemicals, S1049), 10 mM nicotinamide (Sigma, N0626), 20% v/v Wnt-3a conditioned media, and 30% v/v R-spondin1 conditioned media. Wnt-3a and R-spondin1 conditioned media were obtained from the PMLB Facility. PDO cultures were maintained in a Matrigel dome on 24-well plates and cultures were split every 7 to 10 days at a 1:12 splitting ratio. These cells were then harvested on average at day 10 of growth for generation of vascularized organoid tissues on InVADE platform.

2.3. Endothelialization and Organoid Co-Culture on the InVADE Platform

The internal lumen of scaffold on the InVADE platform was first perfused with 0.2% w/v sterile gelatin (Porcine skin, Type A, Sigma) for 2 h at 37 °C to enhance attachment of endothelial cells. The scaffolds were then primed with endothelial growth medium overnight before endothelial cells' seeding. HUVECs were seeded into the lumen of the scaffold through perfusion of concentrated cell suspensions (25×10^6 cells mL^{-1}, 3–5 μL) from both ends of the scaffold. HUVECs were drawn to the luminal scaffold by means of negative pressure and were allowed to attach to the lumen for 1.5 h at 37 °C, followed by flushing of unattached cells with additional endothelial growth media. Perfusion in the InVADE platform was achieved by gravity pressure head between the inlet and outlet wells. Continuous flow in the scaffold was maintained by rocking of the inVADE plate on an automated rocking device with a fixed 20° tilt angle. The flow was reversed every 3 h.

A confluent endothelial layer within the luminal scaffold was achieved with 2–3 d of culture, after which human pancreatic ductal adenocarcinoma (hPDAC) cells derived from PDOs described above were seeded in the parenchymal compartment as single cells and allowed to assemble into vascularized organoid tissue. To facilitate seeding, patient-derived organoid cultures were first dissociated into single cells by incubating with TrypLE Express (Gibco) for 30 min at 37 °C, with repeated mechanical breaking of the Matrigel dome every 10 min. When it appeared under microscopic observation that the majority of the cells were single cells or three- to four-cell clumps, ice-cold advanced DMEM/F12 was added to quench the enzymatic reaction and halt the dissociation process followed by the centrifugation of the cell suspension at $300 \times g$ for 5 min (4 °C). The supernatant was discarded and the patient pancreatic ductal adenocarcinoma cell pellet was re-suspended with ice-cold advanced DMEM/F12 for cell count. Similarly, single-cell suspension of FB was achieved through trypsinization and neutralization with DMEM supplemented with 10% FBS.

Formation of tissue groups (i.e., fibroblast, organoid, and co-culture) in the parenchymal space of InVADE was achieved through Matrigel encapsulation of 1.4×10^4 cells around the polymer vasculature structure. Matrigel cell suspension (1.7×10^6 cells mL^{-1}), 8 μL, was seeded per tissue, except in optimization of the parenchymal tissue seeding density where a lower Matrigel cell suspension concentration (0.85×10^6 cells mL^{-1}, 8 μL per tissue) was used. Fibroblast and organoid tissue groups were composed completely of fibroblasts or tumor cells, respectively. Co-culture tissues were seeded with an equal amount of fibroblasts and tumor cells (50:50). To achieve Matrigel gelation, the InVADE platform was kept at 37 °C for 10 min, followed by the addition of endothelial growth medium to the inlet (500 μL) and outlet wells (20 μL), and OGM (300 μL) to the tissue well (**Figure 1**A). The vascularized organoid tissue was maintained in perfused culture before tissue characterization and drug studies, with media change every 2 days.

2.4. Cell Growth and Organoid Diameter Measurement

The growth of hPDAC on the InVADE platform was measured by quantifying the number of viable cells following seeding as a 3D tissue on scaffolds. Organoid tissues seeded on the polymer tube of the InVADE platform that was either endothelialized or non-endothelialized were subject to CellTiter-Glo 3D (Promega) cell viability luminescent assessment at 1, 2, 4, or 8 days post seeding. OGM media was aspirated from the tissue well and
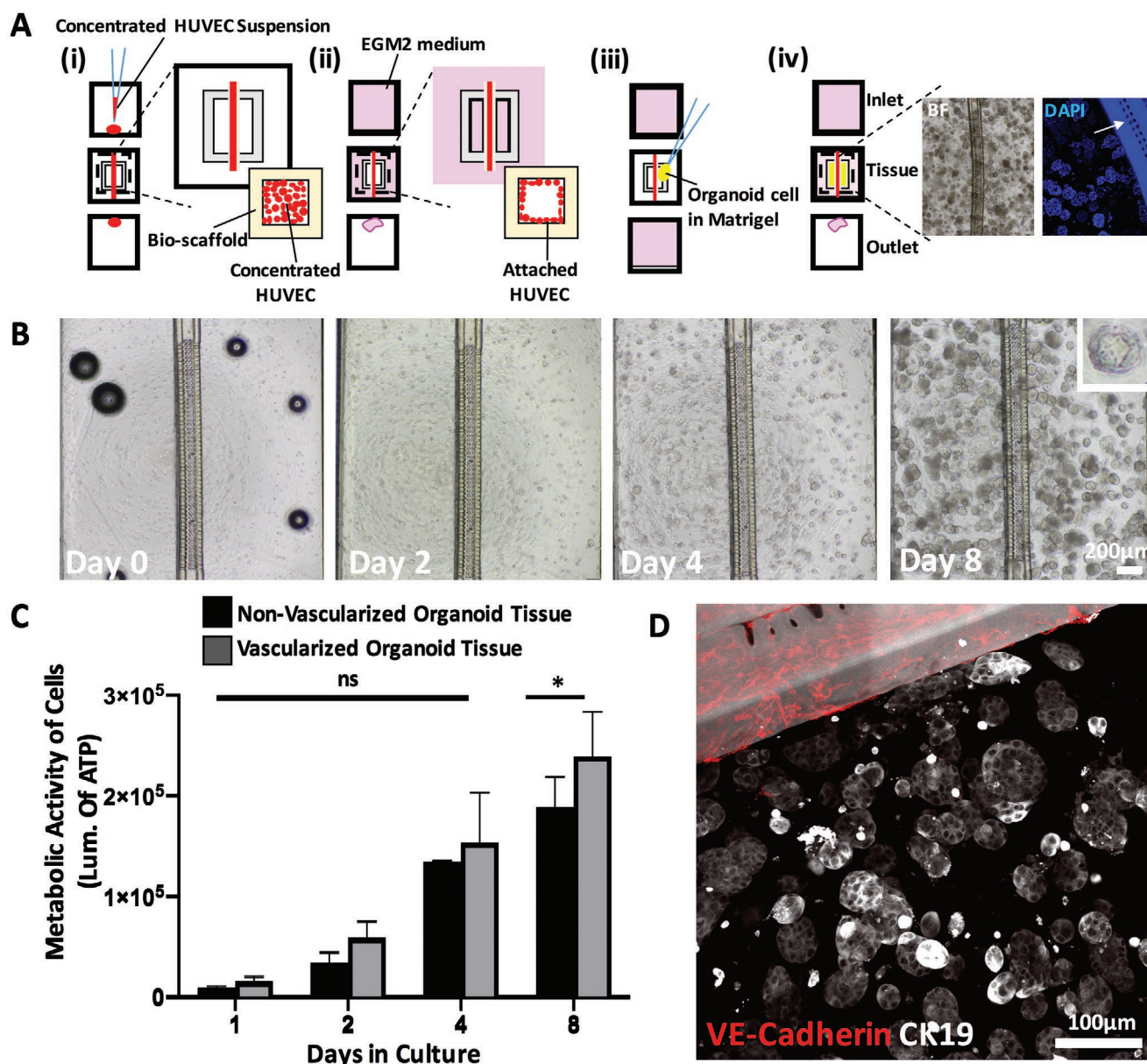
**ADVANCED
SCIENCE NEWS**
www.advancedsciencenews.com

**ADVANCED
FUNCTIONAL
MATERIALS**
www.afm-journal.de

Figure 1. Pancreatic tumor organoids proliferate around endothelialized polymeric vessel of InVADE platform. A) Schematic of cell seeding process on the InVADE platform. i) Endothelializtion of the lumen of the tubular scaffold with HUVEC (red) is performed with addition of concentrated endothelial cell suspension from inlet and outlet of the bio-scaffold (pale yellow). ii) Unattached endothelial cells are removed with perfusion of fresh medium (pink) through a gravity driven flow. iii) Parenchymal cells encapsulated in Matrigel (yellow) are seeded on top of the endothelialized polymeric bio-scaffold. iv) Perfusion is then re-established with application of the gravity driven flow (pink) of cell culture medium. Example of brightfield (BF) and blue fluorescence image (DAPI) illustrate hPDAC-derived organoids around the polymeric vessel. Fluorescence images illustrate the location of micro-holes (arrow) in the vessel wall to facilitate mass transfer. B) Brightfield images of single patient cells cultured into clonally derived organoids over 8 days. Scale bar: 200 µm. C) Metabolic activities of vascularized and non-vascularized organoid tissues over 8 days (data are mean ± SD, *$p < 0.05$, $N = 5$ tissues, two-way ANOVA followed by Tukey's multiple comparison test). D) Immunofluorescence staining of pancreatic epithelium-associated cytokeratin 19 (CK19, white) of the organoid tissue and endothelium of the vascularized InVADE platform vessel (VE-Cadherin, red) on day 8. Polymeric vessel exhibits white autofluorescence. Scale bar: 100 µm.

150 µL of CellTiter-Glo 3D: OGM (2:1) was added to the tissue, followed by mechanical disruption to allow the infiltration of the CellTiter-Glo reagent. Tissues were incubated with shaking (30 min, RT), followed by luminescence capture with Cytation5 Cell Imaging Multi-Mode Reader (BioTek) as a measure of metabolic activity.

To quantify the size of individually formed organoid colonies on InVADE platform and Matrigel Dome study, images of the organoids were acquired using an Olympus CKX52 microscope (4× objective) at the indicated time points. The total number of organoids per tissue was counted 8 days after seeding. Organoid diameter was measured along the long axes using the FIJI

**ADVANCED
SCIENCE NEWS**

www.advancedsciencenews.com

**ADVANCED
FUNCTIONAL
MATERIALS**

www.afm-journal.de

ImageJ software, calibrated against a known scale calibration. Data points of the number and diameter of organoids in both single and co-culture tissues were collected from three tissues per culture condition of two independent experiments.

2.5. Immunostaining and Confocal Microscopy

InVADE tissues were fixed after 8 days in culture (4% paraformaldehyde [PFA], 4 °C, overnight), and then blocked with 10% horse serum and 0.1% Triton-X 100 (1 h, RT). Immunostaining was performed with primary antibodies: rabbit anti-α-smooth muscle actin (Abcam, 1:200, 1 h, RT) and secondary antibody donkey anti-rabbit Alexa Fluor 488 (Abcam; 1:400). Conjugated antibodies of Alexa Fluor 594 anti-cytokeratin 19 (BioLegend; 1:200) were used to stain for CK19. Conjugated vimentin-Cy3 (Sigma; 1:200) was used to stain fibroblasts phenotype prior to use in tissue. Endothelial lining was immunostained with primary antibody rabbit anti-VE-cadherin (Abcam, 1:200, 2 h, RT) and secondary antibody donkey anti-rabbit Alexa Fluor 647 (Abcam, 1:200) or primary antibody mouse anti-CD31 (Abcam, 1:200, 2 h, RT) and secondary antibody goat anti-mouse Alexa Fluor 647 (Abcam, 1:200). DAPI (Invitrogen, 1:1000) was used as a counterstain for each group. Confocal microscopy images were obtained using an Olympus FluoView 1000 laser scanning confocal microscope (Olympus Corporation) at 20× objectives with imaging parameters kept constant for each region.

2.6. Assessment of Collagen Deposition by Two Photon Microscopy

Fixed vascularized organoid tumor tissues were imaged by a second harmonic generation (SHG) laser scanning microscope (Zeiss LSM710 wo-Photon/Confocal microscope). Excitation by two-photon laser (tuned to 840 nm) yielded an SHG signal detectable at a 10 nm wavelength between 395 to 405 nm. To ensure a consistent SHG signal and intrinsic fluorescence intensity, detector offset and gain were set at the consistent values across assessment groups. SHG images were collected as z-stack with a minimum of 15 steps at a step-size of 10 μm. A minimum of three tissues were imaged from each culture group, two regions per tissue. Z-stack images were regenerated with FIJI ImageJ software and the orientation and difference in dispersion of collagen fibers were calculated as area coverage.

2.7. Tissue Elasticity Assessment by Atomic Force Microscopy

Tissue elasticity was measured with a Bruker BioScope Catalyst atomic force microscope (AFM), following 8 days of cultivation. Tissues were first fixed overnight (4 °C, 4% PFA), washed 3 times (phosphate buffered saline [PBS], RT), then secured to cover slips coated with high vacuum grease and hydrated with one drop of PBS. Each AFM indentation measurement was performed using a custom spherio-conical tip manufactured by addition of a 5 μm polystyrene bead to Bruker MLCT-O10 cantilevers. Spring constants were determined using the thermal energy dissipation method as per manufacturer

instructions, wherein cantilevers typically had a spring constant of 0.03 N m^{-1}. Data collected for elasticity was by indentation at a minimum of five spots of ECM in each group of tissues using the contact mode in fluid setting with a trigger force set at 5 nN. A force curve after each indentation was analyzed using the Hertz model following manufacturer protocols.

2.8. Cytokine Release from Vascularized Organoid Tissue

Cytokine concentration was determined in cell supernatants after 8 days of culture using a human focused 13-plex or TGF-β 3-plex ELISA assay (EVE Technologies, Calgary, AB) and calculated using the provided standard curves. The concentrations of cytokines reported (IL-6, MCP-1, and TGF-β1) were normalized to the number of cells in each of the respective tissues. The number of cells in each tissue was estimated by determining the amount of DNA from each tissue and correlating it to a known cell versus DNA standard curve. DNA of cells from each tissue was extracted with a DNeasy Blood & Tissue Kit (Qiagen, 69504), and dsDNA was then quantified with the Quant-iT PicoGreen dsDNA kit (Thermo Fisher, P11496). Both were performed according to manufacturer's instructions.

2.9. Distribution of a Fluorescent Dye in Organoid Tissues

To image a distribution of a fluorescent dye in organoid tissues according to tissue type and the role of perfusion based assessment, 10 μm carboxyfluorescein diacetate (CFDA, MW 557 Da) was perfused through the endothelialized scaffold in InVADE assay and metabolized by live cells in tissue space. Time-lapse fluorescence images were captured at indicated time points (4× objective) with Olympus IX81 microscope fixed in environmental chamber at 37 °C. Binary images were then generated for measuring green fluorescence intensities using Fiji ImageJ software (Figure S3, Supporting Information). The threshold was set at 130 and area coverage above this threshold was reported. A minimum of four tissues from each culture group were analyzed for carboxyfluorescein diacetate (CFDA-SE) perfusion, and three tissues from each culture groups were analyzed for direct CFDA-SE addition.

Food color blue dye (Club House) was mixed at 1 drop per 10 mL of endothelial growth medium and was perfused from inlet well to outlet under gravity driven flow overnight. Amount of dye transferred into the tissue compartment by diffusion after 1.5 and 24 h was determined by measuring the absorbance value of media with the SpectraMax i3 microplate reader (Molecular Devices) at 620 nm, knowing the volume of the media in the tissue compartment to be 300 μL.

2.10. Organoid Tissue Viability under Drug Treatment in InVADE Platform

Vascularized organoid and co-culture tissues were created on InVADE platform as described above. Eight days post-seeding, 1 μm gemcitabine (SelleckChem) in endothelial growth

medium was added to the perfusion media in 3D culture. Four days later (12 d), cell growth was analyzed using CellTiter-Glo 3D as described above.

As static controls, same cell density primary pancreatic organoid and organoid-fibroblast co-culture (≈14 000 total cells on day 0) were seeded as 3D Matrigel domes on a 96-well plate, and similarly treated 8 days post-seeding with 0, 0.01, 0.1, or 1 μm gemcitabine diluted in OGM medium. The cell proliferation of the tissues maintained under static conditions was also assessed using CellTiter-Glo 3D cell proliferation assay (12 days), and the luminescence was captured with Cytation5 Cell Imaging Multi-Mode Reader (Biotek).

Bright-field images of the 4-day drug treatment on both perfused inVADE tissues and static 96-well plate tissues were captured with the Olympus CKX52 microscope (4× objective).

2.11. Statistical Analysis

All bar graph data are presented as the mean ± standard deviation (SD) unless otherwise indicated. Normality and equality of variance were tested before a statistical test. If the normality and equality of variance assumptions were satisfied, significance was measured as indicated for each experiment, either with two-way ANOVA, one-way ANOVA followed by pairwise comparison with Tukey's multiple comparisons test, or a student's t-test using GraphPad Prism 8; $*p < 0.05$, $**p < 0.01$, $***p < 0.001$, $****p < 0.0001$.

3. Results

3.1. Vascularization of Tumor Organoids on InVADE Platform

To adopt features of a human vascularized tumor microenvironment, we used a microfluidic scaffold platform, InVADE, in combination with tumor organoid culture (Figure 1A). The InVADE platform microfluidic scaffold has built in nanopores and microholes as described previously that enable unobstructed transport of molecules and cells across the polymeric scaffold wall.[33] The resulting tumor tissue consists of an endothelialized scaffold lumen (Figure 1A-ii) and Matrigel-encapsulated primary tumor-derived organoids in the parenchymal space (Figure 1A-iv). After 8 days of continuous gravity driven flow culture, the overall coverage of the lumen with endothelial cells is essentially 100%. Representative immunostaining for endothelial markers, CD31, to depict the endothelial coverage is shown in Figure S4, Supporting Information.

To demonstrate that the InVADE platform supports the growth of hPDAC organoids, we seeded single cells into the wells of the InVADE platform and tracked the organoid growth over time. Time-lapse phase contrast imaging of patient derived organoids on InVADE platform showed that many organoids grew from initially seeded single cells by day 8 of culture (Figure 1B). Each single patient cell demonstrated continuous growth and remained metabolically active over the 8-day period (Figure 1C). Vascularized and non-vascularized organoid tissue demonstrated comparable metabolic activity, suggesting endothelialization is non-inhibitory to nutrient delivery and organoid metabolic activity. The patient cells maintained their epithelial phenotype in the organoid form around endothelialized InVADE scaffold lumens, verified through immunostaining for the pancreatic epithelium-associated cytokeratin 19 (CK19) (Figure 1D; Figure S5, Supporting Information).

3.2. Fibroblast Co-Culture Increases Stromal Complexity of Vascularized Organoid Tissues

To study the role of FB as a niche factor in the tumor microenvironment, single pancreatic tumor-derived cells were co-cultured with human FB on the InVADE platform and compared to a tumor-derived cell monoculture. We observed consistently increased compaction of the organoid/FB co-culture tissue (8 days post seeding), compared to the organoid mono-culture tissue. Representative images in **Figure 2**A depict this remodeling of the ECM in all culture groups. Time-lapse phase contrast images presented an inward compaction of the ECM in the organoid/FB co-culture tissue between days 0 and 4, resulting in the pronounced differences between the groups at day 8 as expected. Gel compaction was also evident in monoculture of FB, whereas organoid mono-culture did not exhibit any appreciable signs of matrix remodeling.

We additionally assessed the organoid diameter as an indicator of tumor growth. As expected for tumor tissues, organoid diameters (binned to 5 μm) demonstrated a disperse range in both mono- and co-culture conditions (Figure 2B). Mean organoid diameter in mono-culture tissues was significantly lower (diameter = 24 μm) than that of the co-culture tissues (diameter = 33 μm) (Figure 2C). The difference was further highlighted in a wider distribution of diameters above 30 μm for the co-culture group (Figure 2B). This value was selected as it approximates the median value of the organoid size in the co-culture group. Specifically, 75% of co-cultured organoids were larger than 30 μm in diameter, in contrast to only 40% of mono-cultured organoids above the same threshold. These differences suggest that co-culturing fibroblasts in the tumor organoid environment enhances tumor organoid growth.

On a Matrigel Dome control, after 8 days of cultivation, we also observed a significantly larger size distribution of individual organoids when the human pancreatic organoid single cells are co-cultured with stromal fibroblasts, with a median size of 47 μm in co-culture tissue compared to that of 42 μm in monoculture tissue (Figure S6, Supporting Information). The organoids grown on Matrigel Dome have a larger measured diameter compared to the inVADE grown organoids (Figure S6B, Supporting Information, vs. Figure 2C). This could partially be attributed to the single cells proliferating as two to three organoids fused together. Nevertheless, the size distribution of organoids in both systems shows the symbiotic relationship between the epithelial tumor cells and the stromal cells in co-culture.

It is well known that under certain conditions activated fibroblasts will adopt a myofibroblast phenotype, leading to elevation of collagen ECM and compaction of the matrix architecture, both of which translate to elevated tissue stiffness.[36–40] We therefore looked to assess this behavior in tumor organoid/FB
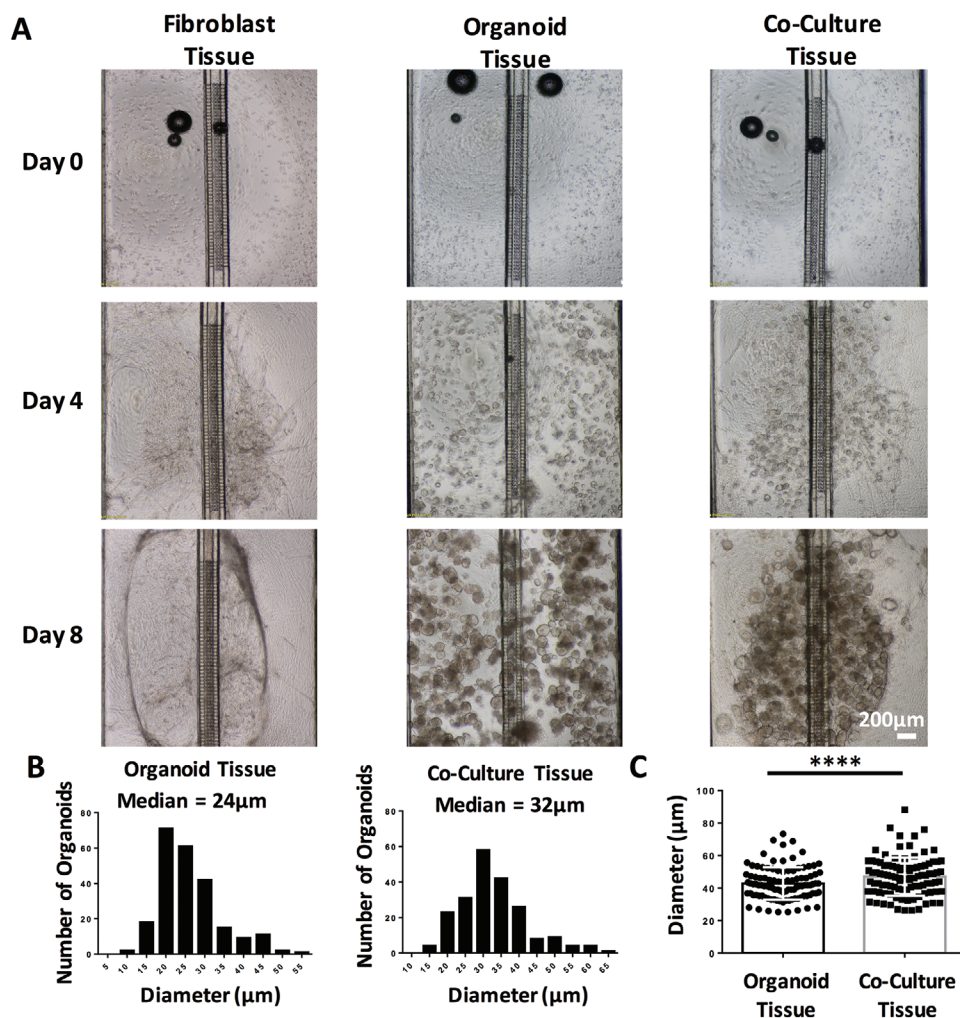
Figure 2. Co-culture of fibroblasts with pancreatic tumor organoids results in dense tissues with larger organoids. A) Brightfield images showing the compaction of extracellular matrix of fibroblast mono-culture control tissue, organoid mono-culture tissue, and organoid/FB co-culture tissues over 8 days. Scale bar: 200 μm. B) Size distribution of individual organoids in organoid tissues and organoid/FB co-culture tissues. C) Average organoid diameter in vascularized organoid tissues and vascularized organoid/FB co-culture tissues (data are mean ± SD, ****$p < 0.0001$, $N = 5$ tissues; tissues were generated from two separate seeding settings; $n = 40$ organoids from each tissues were measured; unpaired student's t-test was used).

microenvironments. Baseline phenotype of FB was determined prior to tissue seeding with single hPDAC-derived cells on the InVADE platform; the FB population stained positive for vimentin and negative for α-SMA, a marker for myofibroblasts (Figure S7, Supporting Information).

To assess FB transition to an activated state in co-culture, we immunostained for α-SMA and CK19, an organoid specific marker. In the dense co-culture tissues, we observed positive staining of α-SMA cells with spindle-like morphology that were dispersed around tumor organoids (**Figure 3**). As expected, our control fibroblast tissues also showed positive staining for α-SMA (Figure 3), which is consistent with other studies reporting on fibroblast-mediated gel compaction, resulting from myofibroblast activation.[41,42] In the organoid tissues, the high magnification images were captured in an area between organoids, depicting the lack of spindle-like cells in the stroma of organoid-only tissue and the abundant presence of α-SMA+ cells in the co-culture stroma. Additionally, consistent with a

previous study,[43] both co-culture and fibroblast tissues exerted a significant tractional force to their surrounding ECM that leads to a significant compaction of the tissues (Figure S8, Supporting Information). However, because of the lack of the myofibroblast subtypes, tumor organoids alone did not exert similar force on their stromal microenvironment. It is interesting to note that the myofibroblasts in the organoid/FB co-culture tissue are only found in close proximity, as symbiotic partners to the epithelial tumor cells in the tumor stroma (Figure S9, Supporting Information).

Given the activated FB phenotype in organoid/FB co-cultures, we assessed the deposition of new collagen (mainly type I) into the surrounding ECM with second harmonic generation microscopy. Co-culture presented a four-fold increase of collagen deposition (**Figure 4**A,B), compared to either organoid-only tissues or FB-only tissue (Figure 4A,B). Importantly, the interactive effects of tumor organoids and FBs in co-culture were evident by the fact that the amount
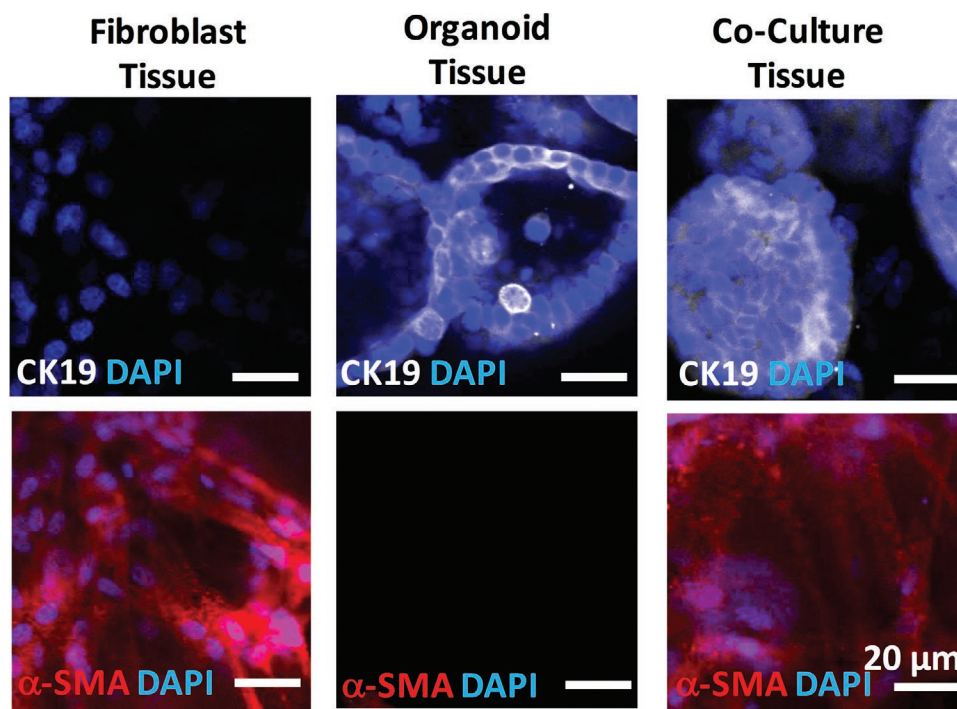
Figure 3. Visualization of fibroblast activation into myofibroblasts. Representative high-magnification confocal images of fibroblast mono-culture tissue, organoid mono-culture tissue, and organoid/FB co-culture tissue after 8 days in culture upon immunostaining for cytokeratin 19 (CK19, white) and α-smooth muscle actin (α-SMA, red). α-SMA staining is visualized in the space between individual organoids. Scale bars: 20 µm.

of collagen in co-culture was not a simple addition of the amount in either monoculture; co-culture tissue presented a sixfold and fivefold increase compared to fibroblast and organoid groups, respectively (Figure 4B). This effect of collagen deposition was also evident in the lower seeding density (0.85×10^6 mL^{-1}) co-culture tissue (Figure S10, Supporting Information, arrows).

Assessment of tissue elasticity further demonstrated the importance of organoid-FB crosstalk. In comparison to Matrigel alone, both organoid and co-culture tissues presented a significant increase in tissue elasticity (Figure 4C), whereas FB-only tissue was comparable to the Matrigel control.

Despite appreciable FB activation in fibroblast control tissues, we did not observe a significant impact on collagen deposition and tissue stiffness to the degree of organoid/FB co-culture tissues. Next, we assessed whether the collagen deposition in the organoid/FB co-culture tissue was a synergistic effect between the cancer organoid cells and the activated fibroblasts. Organoid growth media were collected on day 8 from each of the tissues, and the concentration of cytokines released into the tissue-stromal environment was determined by ELISA (**Figure 5**). A significant increase in the concentration of interleukin-6 (IL-6) and monocyte chemoattractant protein-1 (MCP-1) was observed when pancreatic tumor organoid cells were co-cultured with fibroblasts relative to other culture conditions (Figure 5). Interestingly, transforming growth factor-β1 (TGF-ß1), a well know cytokine responsible for increasing type I collagen deposition in tumor stroma, showed a threefold higher concentration in the fibroblast control tissues, compared to other tissue conditions (Figure 5).

3.3. Tumor Organoid/FB Co-Cultures Exhibit Reduced Uptake of Small Molecules Applied through the Vasculature

To model the distribution of small molecules into a stiffened and remodeled ECM of tumor tissue on the InVADE platform, we perfused 10 µM 557 Da CFDA-SE biomolecule through the vascular scaffold. We imaged the presence of the molecule in the parenchymal space through time-lapse images over the course of 6 h (**Figure 6**). In both the organoid and organoid/FB co-culture tissue groups, the endothelial lumen quickly metabolized CFDA-SE, as the biomolecule was perfused from the inlet well as evidenced by a strong green fluorescence. After 1 h of continuous perfusion, we began to observe green fluorescence in the parenchymal space, indicating that CFDA-SE was able to diffuse into the parenchymal space of the organoid tissues and undergo enzymatic conversion by viable cells (Figure 6A). By the 4 h mark, tumor organoid monocultures were completely fluorescent in green (Figure 6A,B).

In contrast, at the 4 h mark, green fluorescence was only observed around the vascular tube in the tumor organoid/FB co-culture (Figure 6A,B). We observed a significant integrated intensity difference among the two groups of tissues after the 6 h (Figure 6B). Given that metabolic activity assay did not indicate an appreciable difference in cell viability between the two groups (Figure 1C), the reduced green fluorescence is likely consistent with hindered diffusion in the denser matrix of the tumor organoid/FB co-culture group in comparison to the organoids alone.

The limiting resistance to small molecule transfer was further addressed by observing the blue dye diffusion into the
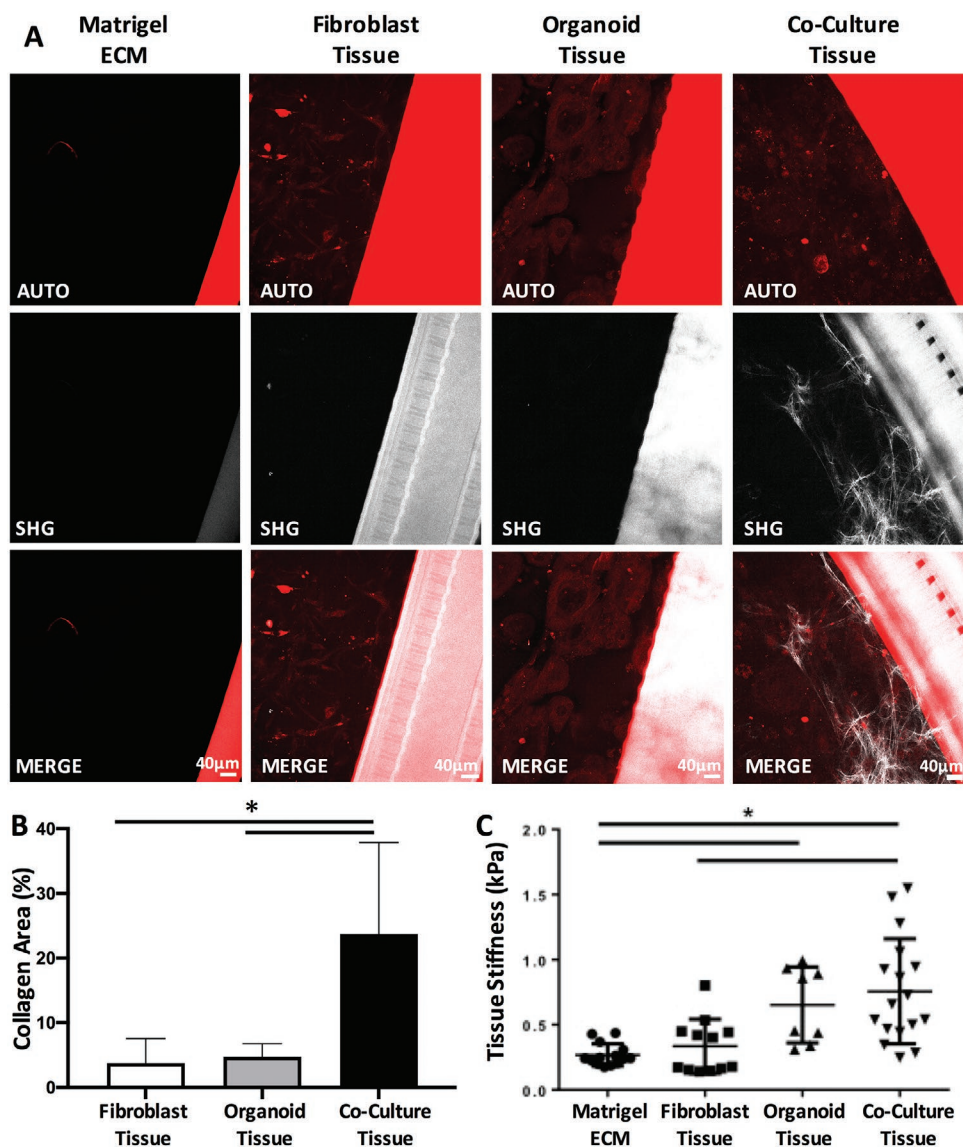
**ADVANCED
SCIENCE NEWS**
www.advancedsciencenews.com

**ADVANCED
FUNCTIONAL
MATERIALS**
www.afm-journal.de

Figure 4. Co-culture of tumor organoids with fibroblasts potentiates pro-fibrotic changes in comparison to monoculture controls. A) Representative second harmonic generation (SHG) images of the Matrigel extracellular matrix, fibroblast mono-culture tissue, organoid mono-culture tissue, and organoid/FB co-culture tissues. Scale bar: 40 µm. B) Quantification of collagen area in each of the tissues measured at day 8 from the second harmonic generation images (data are mean ± SD, *$p < 0.05$, $N = 3$ tissues; z-stack of two different areas of each tissue were imaged; one-way ANOVA followed by Tukey's comparison test). C) Tissue elasticity as determined by atomic force microscopy (data are mean ± SD, *$p < 0.05$, $N = 3$ tissues; minimum of three spots of each tissue; one-way ANOVA, Tukey's comparison test was used).

tissue chamber (Figure S11, Supporting Information). This simple dye does not require enzymatic processing by the cells as CFDA does, thus it therefore decouples diffusion from reaction in the tissue space. Time series of images demonstrates a lower amount of dye transferred into the tissue compartment of the vascularized organoid/FB co-culture tissue, compared to vascularized bio-scaffold alone and vascularized organoid tissue (Figure S11A,B, Supporting Information). Importantly, the bio-scaffold alone did not represent a limiting resistance to the dye transfer, since the amount of the blue dye transferred to the tissue well at 1.5 h of perfusion was already 71% higher compared to the blue dye amount in the tissue compartment of the endothelialized scaffold at 24 h. (Figure S11C, Supporting

Information). The amount of the dye transferred to the tissue compartment in the organoid tissues was higher at 24 h than that of the endothelial cells coated bio-scaffold alone, whereas FB/organoid co-culture resulted in a slightly lower amount of dye transferred compared to the vascularized bio-scaffold (Figure S11D, Supporting Information). After 24 h of dye perfusion, vascularized organoid tissue showed double the amount of dye transferred into tissue space, compared to the co-culture group (Figure S11D, Supporting Information). These findings demonstrate that it is possible to reach high concentration of small molecule in the tissue compartment after an appropriate equilibration time and that the molecule transport is inhibited in the co-culture compared to the organoid group.
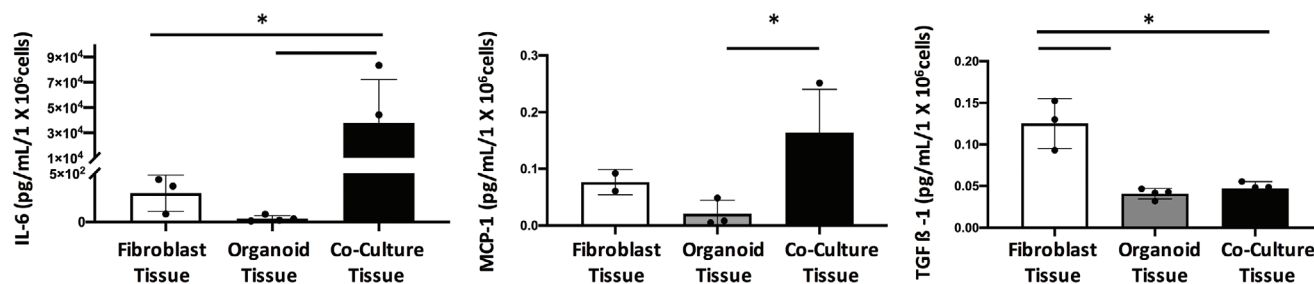
**ADVANCED
SCIENCE NEWS**
www.advancedsciencenews.com

**ADVANCED
FUNCTIONAL
MATERIALS**
www.afm-journal.de

Figure 5. Inflammatory and pro-fibrotic cytokines and chemokines are released in the tissue microenvironment of fibroblast monoculture, organoid monoculture, and organoid/FB co-culture. Results are shown normalized to cell numbers of three biological tissue replicates (data are mean ± SD, *$p < 0.05$, $N = 3$ tissues; one-way ANOVA followed by Tukey's comparison test).

3.4. Inclusion of Vasculature and Stromal Cells Impacts Drug Testing Results in Tumor Organoid Cultures

We assessed the cytotoxic effect of gemcitabine, a standard drug used in the chemotherapeutic treatment for pancreatic ductal adenocarcinoma patients, in tumor organoid and tumor organoid/FB co-culture tissues under static and vasculature perfused conditions. To demonstrate the importance of accurate drug screening process by means of vascular administration, we compared gemcitabine toxicity in each group (FB only, organoid only, organoid/FB co-culture) either cultured as vascularized tissues on InVADE platform (**Figure 7**C) or cultured in Matrigel domes on a static 96-well plate (Figure 7D–F).
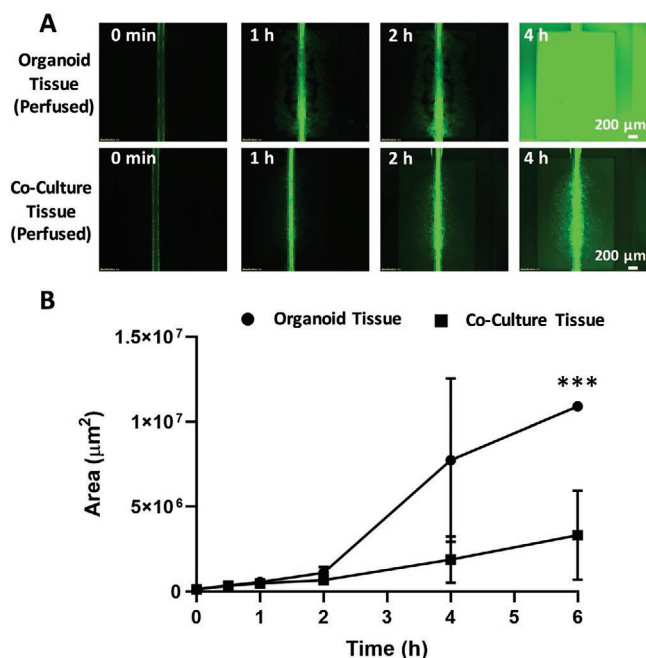

Figure 6. Fibrotic microenvironment of fibroblast/tumor organoid co-cultures hinders transport of small molecules applied through the vasculature. A) Time-lapse fluorescence microscopy images of CFDA-SE distribution in either organoid mono-culture tissue or organoid/FB co-culture tissue. CFDA-SE was perfused from the inlet. Scale bar: 200 µm. B) Quantification of the area of green fluorescence coverage across the tissue chambers for the perfusable viable tissues at 1, 2, 4, and 6 h time points (data are mean ± SD, ***$p < 0.001$, $N = 4$ tissues; unpaired student's t-test was used).

Figure 7A,D depicts the schematic of the tissue formation and drug screening timeline of both treatment groups.

For the perfused treatment group, the organoid/FB co-culture tissues demonstrated an overall higher cell viability after 4 days of treatment at 1 µM of gemcitabine (Figure 7B,C) in comparison to static vasculature free conditions (Figure 7E,F). On the InVADE platform, there were no cytotoxic effects of 1 µM gemcitabine observed in any of the culture groups in comparison to the non-treated controls (Figure 7C). The only observed effect was the morphological change in the organoid monoculture group, with each organoid losing its epithelial glandular cluster of centralized lumen (Figure 7B, inset). In contrast, this morphological change was not observed with the organoid/FB co-culture tissues upon identical drug treatment, suggesting differential microenvironment behavior (Figure 7B, inset).

With direct administration of gemcitabine to the tissue in a static condition, we observed a concentration dependency of drug efficacy and a change in morphology for individual organoids in both organoid monoculture and organoid/FB co-culture groups (Figure 7E,F). This demonstrates differential responses to drugs under static conditions versus perfused endothelialized condition. The higher concentrations of gemcitabine (1 µM) in the organoid/FB co-culture tissue also resulted in a change in the morphological heterogeneity of pancreatic tumor organoid, similar to its effects on organoid mono-cultures and in contrast to the results observed in the vascularized platform where drugs are delivered by perfusion (Figure 7E).

Interestingly, under static conditions, we did not observe a change in the number of viable fibroblast cells in the fibroblast control tissues until the drug concentration reached 1 µM (Figure 7E), and under perfusion in the vascularized inVADE platform, the fibroblast control tissue did not exhibit any decrease in viability (Figure 7C).

4. Discussion

The structural organization of neoplastic cells within tumor tissue determines how these cells function and interact within their surrounding environment. In order to capture the abnormalities of the malignant disease and better replicate tumor behavior than monolayer cultured cells, primary tissue-derived tumor organoids provide an attractive opportunity for studying disease progression.[30,31] However, the lack of an in vivo like stroma and a vascular system within the organoid technology
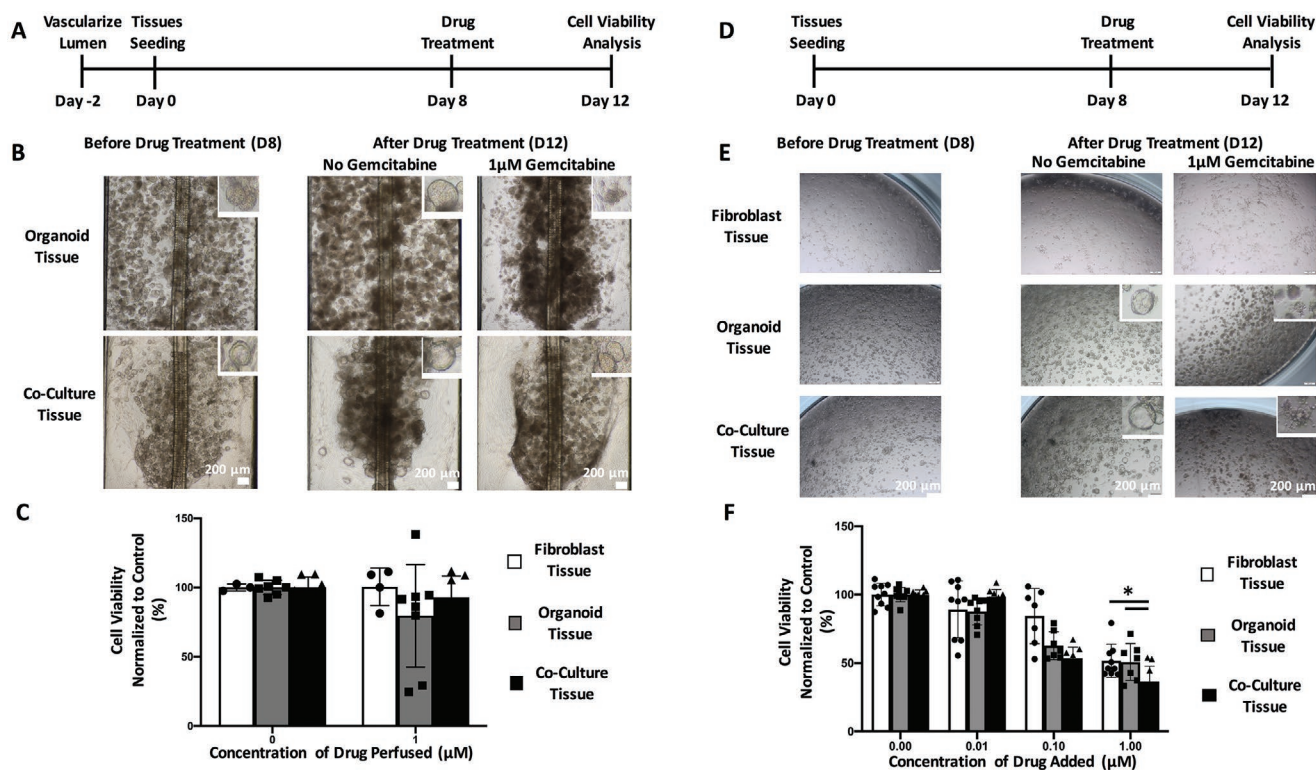
Figure 7. Vascularized fibroblast/organoid co-cultures exhibit reduced chemotherapy drug toxicity in comparison to static 96-well plates. A) Timeline of seeding of vascularized organoid tissues on InVADE platform and the drug application. B) Brightfield images of morphology of vascularized organoid tissues after 4 days of drug perfusion. Scale bar: 200 μm. Insets depict morphological changes to individual organoids after drug treatment. C) Cell viability as measured by CellTiter-Glo on perfused organoid cultures (data are mean ± SD, N = 7 tissues; tissues were generated from three separate seeding settings). D) Timeline of seeding of organoid tissues in co-culture with fibroblasts in a Matrigel dome on a static 96-well plate. E) Brightfield images of morphology of organoid tissues after 4 days of static drug treatment. Scale bar: 200 μm. Insets depict morphological changes to individual organoid after drug treatment. F) Cell viability as measured by CellTiter-Glo on perfused organoid cultures (data are mean ± SD, N = 9 tissues; tissues were generated from three separate seeding settings).

can affect the full investigation of tumor progression and drug resistance.[44] Thus, co-culturing of stromal cells such as fibroblasts and incorporation of a defined perfusable vasculature can provide better understanding to an evolving tumor stroma and its effect on drug bioavailability inside the vascularized tumor tissue. We used InVADE platform due to its documented advantages that include: 1) compatibility with standard imaging and fluid handling technology due to the well plate footprint; 2) ability to run the platform using gravity-driven flow thus removing the need for the pumps and the use of tissue culture plastic for platform fabrication that is expected to decrease drug absorption.

We demonstrated the ability to culture pancreatic patient-derived organoids on our InVADE platform for 8 days as a vascularized tissue and recapitulated in vivo like histological organization of epithelial glandular clusters with either single or multiple lumens, a feature of this patient-derived cell. The open top InVADE system was constructed for the ease of operation since it helps eliminate bubble formation in the lumen of the bio-scaffold and allows for easy interrogation of media (such as cytokine profiling) in the different compartments without disturbing the cells and tissues. This set-up also enables us to address each well independently using simple techniques such as pipetting, which are still currently a standard

in pharmaceutical industry and eliminates the use of pumps which are not widely available in the biological labs. Additionally, we can perform immuno-staining of the 3D tissue simply by detaching the bio-scaffold from the InVADE platform, without disrupting the integrity of the tissue. Also, it is possible to change media in the tissue compartment without stopping the flow in the endothelial compartment. Fortunately, there is no significant direct flow of the medium from the inlet well into the tissue compartment, and the molecules enter that compartment by molecular diffusion as they do in the body. This ensures that there is no additional dilution of the tissue compartment, beyond the volume of 300 μL placed there as we demonstrated in a previous publication.[33]

Furthermore, when the single patient-derived cells were co-cultured with human fibroblasts, we observed a larger size of organoids, suggesting elevated proliferation. This symbiotic interaction between the patient cells and stromal cells is in-line with landmark research reported previously by Ohlund et al. with co-culture of mouse tumor organoids and mouse pancreatic stellate cells.[21] Different from Ohlund et al. organoid disease model, we first dissociated the patient pancreatic organoids into single cells and cultivated these single cells with stromal fibroblasts into the morphologically heterogeneous tumor tissue.

Similar to the work by Ohlund et al., in our modeling of human pancreatic tumor stroma, we also observed banded collagen fibrils deposited in the ECM of the organoid/FB co-culture tissue but limited collagen fibrils in the organoid mono-culture tissue. More importantly, from the second harmonic generation, we were able to confirm these newly deposited collagens in the organoid/FB tissues are of type I collagen origin due to their non-centrosymmetric nature.[45–48] Furthermore, consistent with review contributed by Egeblad et al., these cancer-associated collagens in the organoid/FB co-culture tissue display the thick and linearized assembly rather than adopting the normal "curly" structure.[49] Intriguingly, due to the higher degree of collagen deposition in the ECM and tissue compaction, we were able to demonstrate an increase in tissue stiffness within the organoid/FB co-culture tissue, a phenotypic hallmark of cancer.[50] Thus, the difference of new collagen formation and remodeling in the ECM between the two vascularized organoid tissue groups further justifies the unique role of stromal fibroblasts in studying tumor progression and drug screening with in vitro organoid technology.

It is well reported that the main source of elevated levels of collagen production in tumor stroma are myofibroblasts.[7] Consistent with the description of the synthetic myofibroblasts in PDAC tissues in vitro and in vivo, we observed α-SMA positive cells in fibroblast/organoid co-cultures.[8,21,47] However, when we cultured stromal fibroblasts as a control mono-culture vascularized tissue on InVADE platform in the same organoid growth medium for 8 days, these stromal cells became activated, but interestingly they did not deposit detectable collagen fibrils in the ECM. This may suggest the new type I collagen deposition captured in the co-culture group may result from a symbiotic effect between the neoplastic epithelial cells and the stromal fibroblasts.

It is important to consider additional possible sources of myofibroblast activation, other than the presence of the PDAC tumor organoids. It is possible that fibroblasts could be activated to the myofibroblast phenotype by culture on Matrigel. However, this could be a minor component contributing to the activation observed here, since it has been shown in previous studies that fibroblast-like cell seeded on Matrigel will remain quiescent.[51] More interestingly, both Gaca et al. and Sohara et al. have demonstrated that Matrigel has a reversal effect on myofibroblasts by suppressing the mRNA expression of α–SMA and collagen type I (COL-1A1).[52,53]

Another possible source of myofibroblast activation could be the Wnt3a component in the culture medium. It was previously reported by Carthy et al.[54] that when treated with 250 ng mL^{-1} of recombinant Wnt3a for 24 h, the fibroblasts began to adopt a spindle-like morphology and demonstrated increasing α-SMA expression. However, in their study, they showed that the increased collagen staining was only present within the fibroblast cells and that there was no deposition of collagen into the extracellular matrix nor the formation of banded collagen fibrils.

We attempted to further elucidate these symbiotic effects by investigating the media for the levels of chemokines and cytokines that can lead to a pro-inflammatory and pro-fibrotic microenvironment. Assessing the traditional pro-fibrotic TGF-ß1, we saw a reverse trend where the control fibroblast monoculture tissue had a threefold higher concentration in the media. This difference may stem from the difference in the initial seeding number of stromal fibroblasts between the fibroblast monoculture tissue and organoid/FB co-culture tissue. The initial seeding density was 14 000 single cells encapsulated into 8 µL of Matrigel. By those means, the organoid/FB co-culture tissue only has half the population of fibroblast in comparison that of fibroblast monoculture tissue on day 0. Importantly, the organoid growth media contains TGF-ß1 inhibitor, which may confound these effects. However, we were able to identify two other cytokines, IL-6 and MCP-1, that were significantly upregulated in organoid/FB co-culture tissues. Importantly, IL-6 is a hallmark cytokine secreted in inflammatory fibroblasts of the PDAC microenvironment that was demonstrated to directly mediate tumor survival via JAK/STAT3 pathway.

In other studies, both IL-6 and MCP-1 have also been shown to mediate collagen deposition via either SMAD or JAK/STAT signaling pathway in various fibrosis disease models.[55–60] More importantly, previous work has suggested that both IL-6 and MCP-1 are key regulators on TGF-ß1-induced collagen deposition.[55,58,61] Others have also highlighted the importance of activation of STAT3 signaling by IL-6 in myofibroblasts on the remodeling of the tumor stroma through collagen deposition and disorganization. O'Donoghue et al. have reported that even in the absence of the TGF-ß1 signaling via SMAD3 activation, excessive STAT3 activity can still induce collagen 1a1 genetic transcription to promote lung fibrosis in SMAD3$^{-/-}$ mice group.[62] Similarly, Chakraborty et al. have shown that elevated level of STAT3 activity might be a core mediator of fibrosis through their study on STAT3 comprising fibroblasts being less sensitive to the pro-fibrotic effects of TGF-ß.[63] Furthermore, Xu et al. have indicated the importance of STAT3 activity by demonstrating that TGF-ß1 effect is enhanced through IL-6/STAT3 activity and results in aggravated liver fibrogenesis.[64]

These previous findings may explain why although the stromal fibroblasts are activated and the control fibroblast mono-culture tissue has a higher level of a traditional pro-fibrotic factor, we do not observe collagen deposition in the control tissues, as compared to the organoid/FB co-culture tissues. The excessive fibrillar collagen deposition may be due to a synergistic response of high level of IL-6 and MCP-1 in the organoid/FB co-culture tissue interacting with the TGF-ß1 through both STAT3 and SMAD signaling pathways.

In addition to helping us understanding the evolution of tumor stroma, there is an increasing number of studies correlating the role played by stromal cells on drug resistance.[12,65–69] Thus, the incorporation of stromal fibroblasts into organoid culture could also contribute to the understanding of drug resistance in tumor tissue through the formation of compact matrix and creation of a physical barrier for drug diffusion via increase of intra-tumoral collagen deposition. However, majority of current in vitro drug screening approaches still assess drug effects with the method performed decades ago: direct drug application to 2D or 3D tumor cells. This drug screening method often fails to mimic the actual drug efficacy in vivo, as most drugs are administrated into the tissue space through the vascular systems. To reach tumor, these drugs must diffuse through the endothelium and tumor ECM. Furthermore, because the transport of drugs from vasculature to tumor cells relies upon

diffusion and due to the heterogeneous nature of the tumor microenvironment, not all drug will be completely translocated into the tumor tissue.

In this study, we focused on gemcitabine, the first-line treatment for pancreatic cancer patients in stages II, III, and IV. In some instances, gemcitabine will be used in combination with other chemotherapy agents such as 5-FU or nab-Paclitaxel. It is sold under the name GEMZAR and the standard treatment is administrated through intravenous injection. A number of clinical studies describe the treatment of patients with advanced pancreatic cancer through a constant rate of intravenous infusion of gemcitabine (or in combination with other drugs) under the standard 3 + 3 dose-escalation schema.[70–72] However, gemcitabine has a low retention time in blood, motivating the design of drug delivery systems to solve this problem by means of nanoparticles, liposomes, or albumin.[73–75] It must be noted that pancreatic cancer patients often develop chemo-resistance not because of the endothelial barrier to the drug intravenous administration, but due to the dense fibrous stroma, a hallmark of pancreatic cancer. The dense desmoplastic stroma is often listed as the source of non-cell autonomous contribution that promotes therapeutic resistance.[76–78]

In the case of direct gemcitabine application to the static organoid mono-culture tissues and organoid/FB tissues, we observed the cytotoxic efficacy of the drug over 4 days. However, when we combined the InVADE platform with the organoid technology, we demonstrated the importance of both transport barriers posed by the stroma-protein laden ECM and proper drug delivery through a vascularized tissue. Even when perfusing 1 µM of gemcitabine for a course of 4 days, we did not observe a similar cytotoxic effect as in static application of gemcitabine. A likely explanation for this effect represents the barrier effect to drug distribution across the vascular barrier and a dense stroma of the vascularized tumor tissue. It has been reported that tissue collagen composition alone is unlikely to completely control the resistance to the transport of biomolecules.[79–83] The work performed by Netti et al. has suggested that the combination of proteoglycans and collagen contributes to the interstitial transport resistance.[79] Importantly, our previous work demonstrated physiological permeability of the endothelialized InVADE vessels, proving that the vessel itself was unlikely to profoundly inhibit mass transfer.[33]

It is possible that the cell viability could be slightly different to begin with in InVADE platform versus Matrigel Dome. In the conventional drug studies, the drug concentration is applied in a dose response manner to the cancer cells/tissues by direct exposure, as we have done with the Matrigel Dome experimental condition. However, this is not a true representation of how the drug is administrated in the body. In vivo cancer therapeutic is administered intravenously, where plasma elimination, drug diffusion through the endothelium, and stiffness of an evolving tumor stroma all play significant roles in affecting the drug bioavailability and efficacy.[76–78] Thus, by using the InVADE platform, we are in a position to better mimic two of the listed factors, specifically drug diffusion through the endothelium and stiffness of an evolving tumor stroma.

Here, limiting resistance was further evaluated in the dye transfer study, with all data shown normalized to the amount of blue dye in the tissue compartment of the group consisting of endothelial cells alone. This enables us to benchmark if a certain group has more or less resistance to the dye transfer than the bio-scaffold coated with the endothelial cells. Importantly, the bio-scaffold alone did not represent a limiting resistance to the dye transfer, consistent with our previous report.[33,84] Negligible resistance of the bio-scaffold is afforded by the presence of microholes and nanopores.[33,84] Dye transfer studies additionally demonstrated that the presence of a more relevant cellular environment through the inclusion of fibroblasts can affect the molecule transfer, limiting resistance in the system. These results could also help explain higher efficacy of gemcitabine in the organoid tissue compared to the co-culture tissue. Without any flow, the endothelial cells in the lumen of the bio-scaffold on InVADE platform would die. The death of endothelial cells could cause confounding factors in the drug and small molecule perfusion experiments, and therefore, control without perfusion on the platform was not performed.

Furthermore, the perfusion of 1 µM of gemcitabine over the course of 4 d will not affect the endothelial barrier in the bio-scaffold, as multiple groups have reported gemcitabine only exerts anti-proliferative effect on endothelial cell through cell cycle arrest but does not induce endothelial cell apoptosis.[85,86] Both Laquente et al. and Awasthi et al. have demonstrated that after 24-h direct 500 nM gemcitabine treatment to a confluent HUVEC monolayer, the endothelial cells only exhibited minimal activation of poly(ADP) ribose polymerase cleavage and low level of active caspase-3 on Western blot analysis.[85,86]

Furthermore, the lack of cytotoxicity of gemcitabine in co-culture tissues can also be due to the soluble factor mediated drug resistance as reported by Catelett-Falcone et al., Duan et al., and Franssanito et al. with increasing expression of IL-6.[87–90] In addition to the drug bioavailability through the vasculature and dense ECM playing a role in this work, other factors such as size and shape of organoids and the arrangement within each organoids can also play significant role in interpreting tumor cellular viability.[91]

Limitations of this study include the use of primary human dermal fibroblasts, instead of cancer-associated fibroblasts from pancreatic tumors. We expect the effects on matrix deposition and cytokine secretion to be even more pronounced once cancer-associated fibroblasts are used. Importantly, in line with other studies,[21,22] this work confirms the profound ability of primary hPDAC tumor cells to hijack the functions of naïve fibroblasts for the purpose of creating their own tumor-protective niche by matrix deposition and cytokine secretion. Future studies should also incorporate endothelial cells derived from the pancreatic microvasculature instead of HUVECs.

In summary, we characterized the development of hPDAC tissue microenvironment on the InVADE platform as a vascularized 3D patient-derived pancreatic tumor tissue. We utilized organoid technology and combined it with the bio-scaffold that mimics a perfusable vascularized vessel. In addition, we included human fibroblasts into the culture to act as a prominent player in the remodeling of stroma of the pancreatic tumor tissue. Hallmarks of an evolving tumor tissue stroma such as continuous growth of neoplastic epithelial cells and activation of stromal fibroblasts into myofibroblast symbiotically enhanced cytokine secretion. Remodeling of tumor stiffness through myofibroblast contraction and collagen deposition

were all captured in this disease model. Due to the changes in tumor microenvironment, we also observed a decreased efficacy of gemcitabine when the drug was perfused through the vasculature into the tumor stroma versus direct application of the drug to tumor organoids.

Supporting Information

Supporting Information is available from the Wiley Online Library or from the author.

Acknowledgements

Conflict of Interest

The authors declare no conflict of interest.

Author Contributions

B.F.L.L. and M.R. conceived the idea, designed the experiments, and analyzed the results. B.F.L.L. performed the experiments and analyzed the results. R.X.L. and E.Y.W. assisted in confocal microscopy, organoid culture, and analysis of these results. Y.H. assisted in drug efficacy experiments. L.D.H. synthesized and characterized the polymer materials. W.D. and Y.S. assisted and advised on atomic force microscopy measurements. N.R. and M.S.T. assisted and advised on organoid culture. B.F.L.L., L.D.H., and M.R. wrote the manuscript. M.R. supervised the entire project. All authors read the manuscript, commented on it, and approved its content.

Keywords

[1] R. L. Siegel, K. D. Miller, A. Jemal, *Ca-Cancer J. Clin.* **2016**, *66*, 7.
[2] H. A. Burris 3rd, M. J. Moore, J. Andersen, M. R. Green, M. L. Rothenberg, M. R. Modiano, M. C. Cripps, R. K. Portenoy, A. M. Storniolo, P. Tarassoff, R. Nelson, F. A. Dorr, C. D. Stephens, D. D. Von Hoff, *J. Clin. Oncol.* **1997**, *15*, 2403.
[3] M. Suker, B. R. Beumer, E. Sadot, L. Marthey, J. E. Faris, E. A. Mellon, B. F. El-Rayes, A. Wang-Gillam, J. Lacy, P. J. Hosein, S. Y. Moorcraft, T. Conroy, F. Hohla, P. Allen, J. Taieb, T. S. Hong, R. Shridhar, I. Chau, C. H. van Eijck, B. G. Koerkamp, *Lancet Oncol.* **2016**, *17*, 801.
[4] S. C. Lau, W. Y. Cheung, *World J. Gastro. Oncol.* **2017**, *9*, 281.
[5] D. P. Ryan, T. S. Hong, N. Bardeesy, *N. Engl. J. Med.* **2014**, *371*, 1039.
[6] S. K. Dougan, *Cancer J.* **2017**, *23*, 321.
[7] R. Kalluri, *Nat. Rev. Cancer* **2016**, *16*, 582.
[8] M. Ligorio, S. Sil, J. Malagon-Lopez, L. T. Nieman, S. Misale, M. Di Pilato, R. Y. Ebright, M. N. Karabacak, A. S. Kulkarni, A. Liu, N. Vincent Jordan, J. W. Franses, J. Philipp, J. Kreuzer, N. Desai, K. S. Arora, M. Rajurkar, E. Horwitz, A. Neyaz, E. Tai, N. K. C. Magnus, K. D. Vo, C. N. Yashaswini, F. Marangoni, M. Boukhali, J. P. Fatherree, L. J. Damon, K. Xega, R. Desai, M. Choz, et al., *Cell* **2019**, *178*, 160.
[9] D. Pankova, Y. Chen, M. Terajima, M. J. Schliekelman, B. N. Baird, M. Fahrenholtz, L. Sun, B. J. Gill, T. J. Vadakkan, M. P. Kim, Y. H. Ahn, J. D. Roybal, X. Liu, E. R. Parra Cuentas, J. Rodriguez, I. I. Wistuba, C. J. Creighton, D. L. Gibbons, J. M. Hicks, M. E. Dickinson, J. L. West, K. J. Grande-Allen, S. M. Hanash, M. Yamauchi, J. M. Kurie, *Mol. Cancer Res.* **2016**, *14*, 287.
[10] C. Feig, J. O. Jones, M. Kraman, R. J. Wells, A. Deonarine, D. S. Chan, C. M. Connell, E. W. Roberts, Q. Zhao, O. L. Caballero, S. A. Teichmann, T. Janowitz, D. I. Jodrell, D. A. Tuveson, D. T. Fearon, *Proc. Natl. Acad. Sci. USA* **2013**, *110*, 20212.
[11] K. E. Richards, A. E. Zeleniak, M. L. Fishel, J. Wu, L. E. Littlepage, R. Hill, *Oncogene* **2017**, *36*, 1770.
[12] L. Wei, H. Ye, G. Li, Y. Lu, Q. Zhou, S. Zheng, Q. Lin, Y. Liu, Z. Li, R. Chen, *Cell Death Dis.* **2018**, *9*, 1065.
[13] A. Ene-Obong, A. J. Clear, J. Watt, J. Wang, R. Fatah, J. C. Riches, J. F. Marshall, J. Chin-Aleong, C. Chelala, J. G. Gribben, A. G. Ramsay, H. M. Kocher, *Gastroenterology* **2013**, *145*, 1121.
[14] T. Armstrong, G. Packham, L. B. Murphy, A. C. Bateman, J. A. Conti, D. R. Fine, C. D. Johnson, R. C. Benyon, J. P. Iredale, *Clin. Cancer Res.* **2004**, *10*, 7427.
[15] N. Hartmann, N. A. Giese, T. Giese, I. Poschke, R. Offringa, J. Werner, E. Ryschich, *Clin. Cancer Res.* **2014**, *20*, 3422.
[16] B. Garg, B. Giri, S. Modi, V. Sethi, I. Castro, O. Umland, Y. Ban, S. Lavania, R. Dawra, S. Banerjee, S. Vickers, N. B. Merchant, S. X. Chen, E. Gilboa, S. Ramakrishnan, A. Saluja, V. Dudeja, *Gastroenterology* **2018**, *155*, 880.
[17] B. C. Ozdemir, T. Pentcheva-Hoang, J. L. Carstens, X. Zheng, C. C. Wu, T. R. Simpson, H. Laklai, H. Sugimoto, C. Kahlert, S. V. Novitskiy, A. De Jesus-Acosta, P. Sharma, P. Heidari, U. Mahmood, L. Chin, H. L. Moses, V. M. Weaver, A. Maitra, J. P. Allison, V. S. LeBleu, R. Kalluri, *Cancer Cell* **2014**, *25*, 719.
[18] E. J. Kim, V. Sahai, E. V. Abel, K. A. Griffith, J. K. Greenson, N. Takebe, G. N. Khan, J. L. Blau, R. Craig, U. G. Balis, M. M. Zalupski, D. M. Simeone, *Clin. Cancer Res.* **2014**, *20*, 5937.
[19] C. M. Sousa, D. E. Biancur, X. Wang, C. J. Halbrook, M. H. Sherman, L. Zhang, D. Kremer, R. F. Hwang, A. K. Witkiewicz, H. Ying, J. M. Asara, R. M. Evans, L. C. Cantley, C. A. Lyssiotis, A. C. Kimmelman, *Nature* **2016**, *536*, 479.
[20] S. Y. Jeong, J. H. Lee, Y. Shin, S. Chung, H. J. Kuh, *PLoS One* **2016**, *11*, e0159013.
[21] D. Ohlund, A. Handly-Santana, G. Biffi, E. Elyada, A. S. Almeida, M. Ponz-Sarvise, V. Corbo, T. E. Oni, S. A. Hearn, E. J. Lee, I. I. C. Chio, C.-i. Hwang, H. Tiriac, L. A. Baker, D. D. Engle, C. Feig, A. Kultti, M. Egeblad, D. T. Fearon, J. M. Crawford, H. Clevers, Y. Park, D. A. Tuveson, *J. Exp. Med.* **2017**, *214*, 579.
[22] G. Lazzari, V. Nicolas, M. Matsusaki, M. Akashi, P. Couvreur, S. Mura, *Acta Biomater.* **2018**, *78*, 296.
[23] F. R. Auciello, V. Bulusu, C. Oon, J. Tait-Mulder, M. Berry, S. Bhattacharyya, S. Tumanov, B. L. Allen-Petersen, J. Link, N. D. Kendsersky, E. Vringer, M. Schug, D. Novo, R. F. Hwang, R. M. Evans, C. Nixon, C. Dorrell, J. P. Morton, J. C. Norman, R. C. Sears, J. J. Kamphorst, M. H. Sherman, *Cancer Discovery* **2019**, *9*, 617.

[24] W.-H. Jung, N. Yam, C.-C. Chen, K. Elawad, B. Hu, Y. Chen, *Biomaterials* **2020**, *234*, 119756.

[25] S. Nagaraju, D. Truong, G. Mouneimne, M. Nikkhah, *Adv. Healthcare Mater.* **2018**, *7*, 1701257.

[26] H. Saini, K. R. Eliato, J. Veldhuizen, A. Zare, M. Allam, C. Silva, A. Kratz, D. Truong, G. Mouneimne, J. LaBaer, R. Ros, M. Nikkhah, *Biomaterials* **2020**, *247*, 119975.

[27] S. P. Lamichhane, N. Arya, E. Kohler, S. Xiang, J. Christensen, V. P. Shastri, *BMC Cancer* **2016**, *16*, 581.

[28] A. Amann, M. Zwierzina, S. Koeck, G. Gamerith, E. Pechriggl, J. M. Huber, E. Lorenz, J. M. Kelm, W. Hilbe, H. Zwierzina, J. Kern, *Sci. Rep.* **2017**, *7*, 2963.

[29] B. Weigelt, C. M. Ghajar, M. J. Bissell, *Adv. Drug Delivery Rev.* **2014**, *69–70*, 42.

[30] D. Dutta, I. Heo, H. Clevers, *Trends Mol. Med.* **2017**, *23*, 393.

[31] M. A. Lancaster, J. A. Knoblich, *Science* **2014**, *345*, 1247125.

[32] T. Takebe, B. Zhang, M. Radisic, *Cell Stem Cell* **2017**, *21*, 297.

[33] B. F. L. Lai, L. Davenport Huyer, R. X. Z. Lu, S. Drecun, M. Radisic, B. Zhang, *Adv. Funct. Mater.* **2017**, *27*, 1703524.

[34] L. Davenport Huyer, B. Zhang, A. Korolj, M. Montgomery, S. Drecun, G. Conant, Y. Zhao, L. Reis, M. Radisic, *ACS Biomater. Sci. Eng.* **2016**, *2*, 780.

[35] S. F. Boj, C. I. Hwang, L. A. Baker, I. I. C. Chio, D. D. Engle, V. Corbo, M. Jager, M. Ponz-Sarvise, H. Tiriac, M. S. Spector, A. Gracanin, T. Oni, K. H. Yu, R. van Boxtel, M. Huch, K. D. Rivera, J. P. Wilson, M. E. Feigin, D. Ohlund, A. Handly-Santana, C. M. Ardito-Abraham, M. Ludwig, E. Elyada, B. Alagesan, G. Biffi, G. N. Yordanov, B. Delcuze, B. Creighton, K. Wright, Y. Park, et al., *Cell* **2015**, *160*, 324.

[36] C. C. DuFort, M. J. Paszek, V. M. Weaver, *Nat. Rev. Mol. Cell Biol.* **2011**, *12*, 308.

[37] C. P. Ng, B. Hinz, M. A. Swartz, *J. Cell Sci.* **2005**, *118*, 4731.

[38] G. S. Karagiannis, T. Poutahidis, S. E. Erdman, R. Kirsch, R. H. Riddell, E. P. Diamandis, *Mol. Cancer Res.* **2012**, *10*, 1403.

[39] A. J. Rice, E. Cortes, D. Lachowski, B. C. H. Cheung, S. A. Karim, J. P. Morton, A. Del Rio Hernandez, *Oncogenesis* **2017**, *6*, e352.

[40] D. Lachowski, E. Cortes, D. Pink, A. Chronopoulos, S. A. Karim, J. P. Morton, A. E. del Rio Hernandez, *Sci. Rep.* **2017**, *7*, 2506.

[41] E. Tamariz, F. Grinnell, *Mol. Biol. Cell* **2002**, *13*, 3915.

[42] Z. Feng, Y. Wagatsuma, M. Kikuchi, T. Kosawada, T. Nakamura, D. Sato, N. Shirasawa, T. Kitajima, M. Umezu, *Biomaterials* **2014**, *35*, 8078.

[43] H. Saini, K. Rahmani Eliato, C. Silva, M. Allam, G. Mouneimne, R. Ros, M. Nikkhah, *Cell Mol. Bioeng.* **2018**, *11*, 419.

[44] S. E. Park, A. Georgescu, D. Huh, *Science* **2019**, *364*, 960.

[45] S. Ranjit, A. Dvornikov, M. Stakic, S. H. Hong, M. Levi, R. M. Evans, E. Gratton, *Sci. Rep.* **2015**, *5*, 13378.

[46] X. Chen, O. Nadiarynkh, S. Plotnikov, P. J. Campagnola, *Nat. Protoc.* **2012**, *7*, 654.

[47] C. J. Hanley, F. Noble, M. Ward, M. Bullock, C. Drifka, M. Mellone, A. Manousopoulou, H. E. Johnston, A. Hayden, S. Thirdborough, Y. Liu, D. M. Smith, T. Mellows, W. J. Kao, S. D. Garbis, A. Mirnezami, T. J. Underwood, K. W. Eliceiri, G. J. Thomas, *Oncotarget* **2016**, *7*, 6159.

[48] C. R. Drifka, A. G. Loeffler, K. Mathewson, G. Mehta, A. Keikhosravi, Y. Liu, S. Lemancik, W. A. Ricke, S. M. Weber, W. J. Kao, K. W. Eliceiri, *J. Histochem. Cytochem.* **2016**, *64*, 519.

[49] M. Egeblad, M. G. Rasch, V. M. Weaver, *Curr. Opin. Cell Biol.* **2010**, *22*, 697.

[50] K. R. Levental, H. Yu, L. Kass, J. N. Lakins, M. Egeblad, J. T. Erler, S. F. Fong, K. Csiszar, A. Giaccia, W. Weninger, M. Yamauchi, D. L. Gasser, V. M. Weaver, *Cell* **2009**, *139*, 891.

[51] S. L. Friedman, F. J. Roll, J. Boyles, D. M. Arenson, D. M. Bissell, *J. Biol. Chem.* **1989**, *264*, 10756.

[52] M. D. Gaca, X. Zhou, R. Issa, K. Kiriella, J. P. Iredale, R. C. Benyon, *Matrix Biol.* **2003**, *22*, 229.

[53] N. Sohara, I. Znoyko, M. T. Levy, M. Trojanowska, A. Reuben, *J. Hepatol.* **2002**, *37*, 214.

[54] J. M. Carthy, F. S. Garmaroudi, Z. Luo, B. M. McManus, *PLoS One* **2011**, *6*, e19809.

[55] S. O'Reilly, M. Ciechomska, R. Cant, J. M. van Laar, *J. Biol. Chem.* **2014**, *289*, 9952.

[56] G. Zhao, G. Zhu, Y. Huang, W. Zheng, J. Hua, S. Yang, J. Zhuang, J. Ye, *Oncol. Rep.* **2016**, *35*, 1787.

[57] Q. Zhu, X. Zhang, L. Zhang, W. Li, H. Wu, X. Yuan, F. Mao, M. Wang, W. Zhu, H. Qian, W. Xu, *Cell Death Dis.* **2014**, *5*, e1295.

[58] A. M. Dufour, M. Alvarez, B. Russo, C. Chizzolini, *Front. Immunol.* **2018**, *9*, 1865.

[59] M. Gharaee-Kermani, E. M. Denholm, S. H. Phan, *J. Biol. Chem.* **1996**, *271*, 17779.

[60] T. Yamamoto, K. Hartmann, B. Eckes, T. Krieg, *J. Dermatol. Sci.* **2001**, *26*, 106.

[61] X. L. Zhang, N. Topley, T. Ito, A. Phillips, *J. Biol. Chem.* **2005**, *280*, 12239.

[62] R. J. J. O'Donoghue, D. A. Knight, C. D. Richards, C. M. Prele, H. L. Lau, A. G. Jarnicki, J. Jones, S. Bozinovski, R. Vlahos, S. Thiem, B. S. McKenzie, B. Wang, P. Stumbles, G. J. Laurent, R. J. McAnulty, S. Rose-John, H. J. Zhu, G. P. Anderson, M. R. Ernst, S. E. Mutsaers, *EMBO Mol. Med.* **2012**, *4*, 939.

[63] D. Chakraborty, B. Sumova, T. Mallano, C. W. Chen, A. Distler, C. Bergmann, I. Ludolph, R. E. Horch, K. Gelse, A. Ramming, O. Distler, G. Schett, L. Senolt, J. H. W. Distler, *Nat. Commun.* **2017**, *8*, 1130.

[64] M.-Y. Xu, J.-J. Hu, J. Shen, M.-L. Wang, Q.-Q. Zhang, Y. Qu, L.-G. Lu, *Biochim. Biophys. Acta, Mol. Basis Dis.* **2014**, *1842*, 2237.

[65] Y. Kinugasa, T. Matsui, N. Takakura, *Stem Cells* **2014**, *32*, 145.

[66] C. Duluc, S. Moatassim-Billah, M. Chalabi-Dchar, A. Perraud, R. Samain, F. Breibach, M. Gayral, P. Cordelier, M. B. Delisle, M. P. Bousquet-Dubouch, R. Tomasini, H. Schmid, M. Mathonnet, S. Pyronnet, Y. Martineau, C. Bousquet, *EMBO Mol. Med.* **2015**, *7*, 735.

[67] M. J. Ware, V. Keshishian, J. J. Law, J. C. Ho, C. A. Favela, P. Rees, B. Smith, S. Mohammad, R. F. Hwang, K. Rajapakshe, C. Coarfa, S. Huang, D. P. Edwards, S. J. Corr, B. Godin, S. A. Curley, *Biomaterials* **2016**, *108*, 129.

[68] J. H. Lee, S. K. Kim, I. A. Khawar, S. Y. Jeong, S. Chung, H. J. Kuh, *J. Exp. Clin. Cancer Res.* **2018**, *37*, 4.

[69] Y. Shintani, A. Fujiwara, T. Kimura, T. Kawamura, S. Funaki, M. Minami, M. Okumura, *J. Thorac. Oncol.* **2016**, *11*, 1482.

[70] D. D. Von Hoff, R. K. Ramanathan, M. J. Borad, D. A. Laheru, L. S. Smith, T. E. Wood, R. L. Korn, N. Desai, V. Trieu, J. L. Iglesias, H. Zhang, P. Soon-Shiong, T. Shi, N. V. Rajeshkuman, A. Maitra, M. Hidalgo, *J. Clin. Oncol.* **2011**, *29*, 4548.

[71] A. H. Ko, T. G. Truong, E. Kantoff, K. A. Jones, E. Dito, A. Ong, M. A. Tempero, *Cancer Chemother. Pharmacol.* **2012**, *70*, 875.

[72] F. Di Costanzo, P. Carlini, L. Doni, B. Massidda, R. Mattioli, A. Iop, E. Barletta, L. Moscetti, F. Recchia, P. Tralongo, S. Gasperoni, *Br. J. Cancer* **2005**, *93*, 185.

[73] J. Y. Park, Y. L. Cho, J. R. Chae, S. H. Moon, W. G. Cho, Y. J. Choi, S. J. Lee, W. J. Kang, *Mol. Ther. Nucleic Acids* **2018**, *12*, 543.

[74] D. Chitkara, A. Mittal, S. W. Behrman, N. Kumar, R. I. Mahato, *Bioconjugate Chem.* **2013**, *24*, 1161.

[75] J. Li, Y. Di, C. Jin, D. Fu, F. Yang, Y. Jiang, L. Yao, S. Hao, X. Wang, S. Subedi, Q. Ni, *Nanoscale Res. Lett.* **2013**, *8*, 176.

[76] A. Dimou, K. N. Syrigos, M. W. Saif, *Ther. Adv. Med. Oncol.* **2012**, *4*, 271.

[77] I. M. Stromnes, K. E. DelGiorno, P. D. Greenberg, S. R. Hingorani, *Carcinogenesis* **2014**, *35*, 1451.

[78] P. P. Adiseshaiah, R. M. Crist, S. S. Hook, S. E. McNeil, *Nat. Rev. Clin. Oncol.* **2016**, *13*, 750.

**ADVANCED
SCIENCE NEWS**

www.advancedsciencenews.com

**ADVANCED
FUNCTIONAL
MATERIALS**

www.afm-journal.de

[79] P. A. Netti, D. A. Berk, M. A. Swartz, A. J. Grodzinsky, R. K. Jain, *Cancer Res.* **2000**, *60*, 2497.

[80] C. Voutouri, C. Polydorou, P. Papageorgis, V. Gkretsi, T. Stylianopoulos, *Neoplasia* **2016**, *18*, 732.

[81] C. Voutouri, T. Stylianopoulos, *PLoS One* **2018**, *13*, e0193801.

[82] N. N. Rahbari, D. Kedrin, J. Incio, H. Liu, W. W. Ho, H. T. Nia, C. M. Edrich, K. Jung, J. Daubriac, I. Chen, T. Heishi, J. D. Martin, Y. Huang, N. Maimon, C. Reissfelder, J. Weitz, Y. Boucher, J. W. Clark, A. J. Grodzinsky, D. G. Duda, R. K. Jain, D. Fukumura, *Sci. Transl. Med.* **2016**, *8*, 360ra135.

[83] M. A. Jacobetz, D. S. Chan, A. Neesse, T. E. Bapiro, N. Cook, K. K. Frese, C. Feig, T. Nakagawa, M. E. Caldwell, H. I. Zecchini, M. P. Lolkema, P. Jiang, A. Kultti, C. B. Thompson, D. C. Maneval, D. I. Jodrell, G. I. Frost, H. M. Shepard, J. N. Skepper, D. A. Tuveson, *Gut* **2013**, *62*, 112.

[84] B. Zhang, M. Montgomery, M. D. Chamberlain, S. Ogawa, A. Korolj, A. Pahnke, L. A. Wells, S. Masse, J. Kim, L. Reis, A. Momen, S. S. Nunes, A. R. Wheeler, K. Nanthakumar, G. Keller, M. V. Sefton, M. Radisic, *Nat. Mater.* **2016**, *15*, 669.

[85] B. Laquente, C. Lacasa, M. M. Ginesta, O. Casanovas, A. Figueras, M. Galan, I. G. Ribas, J. R. Germa, G. Capella, F. Vinals, *Mol. Cancer Ther.* **2008**, *7*, 638.

[86] N. Awasthi, C. Zhang, S. Hinz, M. A. Schwarz, R. E. Schwarz, *J. Exp. Clin. Cancer Res.* **2013**, *32*, 12.

[87] R. Catlett-Falcone, T. H. Landowski, M. M. Oshiro, J. Turkson, A. Levitzki, R. Savino, G. Ciliberto, L. Moscinski, J. L. Fernandez-Luna, G. Nunez, W. S. Dalton, R. Jove, *Immunity* **1999**, *10*, 105.

[88] Z. Duan, D. E. Lamendola, R. T. Penson, K. M. Kronish, M. V. Seiden, *Cytokine* **2002**, *17*, 234.

[89] D. Conze, L. Weiss, P. S. Regen, A. Bhushan, D. Weaver, P. Johnson, M. Rincon, *Cancer Res.* **2001**, *61*, 8851.

[90] M. A. Frassanito, A. Cusmai, G. Iodice, F. Dammacco, *Blood* **2001**, *97*, 483.

[91] J. A. Brassard, M. P. Lutolf, *Cell Stem Cell* **2019**, *24*, 860.